Case Studies in Thermal Engineering 6 (2015) 16–27

Contents lists available at ScienceDirect

Case Studies in Thermal Engineering

journal homepage: www.elsevier.com/locate/csite

Numerical study on electromagnetics and thermal cooling of a switched reluctance motor

Jer-Huan Jang [a], Han-Chieh Chiu [b], Wei-Mon Yan [c,*], M.C. Tsai [d], Pin-Yuan Wang [d]

[a] Department of Mechanical Engineering, Ming Chi University of Technology, Taishan, New Taipei City 243, Taiwan
[b] Department of Mechanical Engineering, Taipei City University of Science and Technology, Peitou, Taipei 112, Taiwan
[c] Department of Energy and Refrigerating Air-Conditioning Engineering, National Taipei University of Technology, Taipei 106, Taiwan
[d] Electric Motors Technology Research Center, National Cheng Kung University, Tainan 701, Taiwan

ARTICLE INFO

Article history:
Received 10 March 2015
Received in revised form
7 May 2015
Accepted 9 May 2015
Available online 13 May 2015

Keywords:
Switched reluctance motor
Electro-magnetic behavior
Thermal design
Efficiency improvement

ABSTRACT

In this study, the coupled thermomagnetic system of a switched reluctance motor for cooling performance improvement has been conducted numerically. The switched reluctance motor (SRM) with output power of 3 kW and air cooling is under investigation. Aluminum cooling fins are fitted on the cooling casing of the motor in order to increase the convection surfaces. The commercial softwares used in this paper are JMAG-Designer and CFD-RC for electromagnetic field and thermal field analyzes, respectively. The electromagnetic analysis for the switched reluctance motor is obtained in advanced in order to obtain the energy losses. They can then be treated as the heat sources for heat transfer analysis. Transient solutions for the temperatures of the components in SRM are calculated during operation. The transient temperature of SRM is analyzed for both with and without cooling casing. The influence of forced convection by the internal fan of the SRM is also under investigation. Results show the numerical model is in good agreement to the real practice. The model can be used for the SRM cooling design.

1. Introduction

Electric motors are widely used in industrial applications. Especially in recent years, electric or hybrid vehicles have been developed due to environmental issues and energy problems. Electromagnetic field analysis has been developed to a practical level for motor design. Rahman et al. [1] investigated the capabilities of the switched reluctance motor (SRM) for electric vehicle and hybrid electric vehicle applications. Nakamura et al. [2] presented a reluctance network analysis (RNA) model of a switched reluctance motor considering iron loss. Ohyama et al. [3] used finite-element method (FEM) in estimating the static torque of SRM with the magnetic field analysis. They found the 60 kW SRM employed in EV, whose output characteristics are equal to 1500 cc gasoline engine. Fulton [4] and Miller and McGilp [5] have been developed software programs in designing SRM based on the empirical modeling of the geometry and magnetic circuits. Kakilli [6] had modeled a 3-phase, 12/8-pole, modified-rotor switched reluctance motor with rotor helical method having a right geometry in 3-D environment for the magnetic analysis using FEM. Li et al. [7] presented copper and iron loss models of a classical SRM and a mutually coupled SRM (MCSRM). A comparison between the maximum temperatures obtained by using different heat source (average power losses or instantaneous power losses during driving cycles) is given. Their numerical results have

* Corresponding author.
E-mail address: wmyan@ntut.edu.tw (P.-Y. Wang).

http://dx.doi.org/10.1016/j.csite.2015.05.001

Nomenclature

B	friction coefficient of the motor with loading
C_p	specific heat
e	counter electromotive force
h	convection coefficient
i	current
J	rotational momentum of the motor with loading
k	thermal conductivity
L	inductance of the coil winding section
p	pressure
P	power loss
$\dot{q}$	heat generation rate per solid volume
R	coil winding resistance
T	temperature
T_e	torque produced by the motor
T_L	torque of the loading
t	time
V	voltage
u, v, w	velocity in x, y, z direction
x, y, z	direction

Greek

θ_r	rotational angle of the motor
μ	dynamic viscosity
ρ	density
ω_r	rotational speed

Subscription

Copper	of copper
in	inside the motor
f	of working fluid
out	outside the motor
rotor	of rotor
s	of the solid
stator	of stator
x	in x-phase

shown that the copper losses of the MCSRM are much lower than those of classical SRM during the same driving cycle. Concerning the iron losses, the MCSRM has lower stator as well as rotor iron losses than those of the classical SRM for the same driving cycle.

However, cooling of electric motors is a critical problem in the motor design and manufacturing industry because of heat generation by the motor. In addition, the temperature rise could cause the deterioration of insulation in windings. Motor efficiency decreases as temperature increases with increasing energy loss. It is realized that the design of motors should not only be focused on electric matters, but also control of all different disciplines of electrodynamics, thermodynamics, metallurgy, chemistry, static and dynamic strength of structures [8]. Faiz et al. [9] proposed a lumped-parameter approach for prediction of the steady-state and transient thermal behavior of a prototype multiple teeth per stator pole switched reluctance motor of TEFC (Totally Enclosed fan-cooled) design and experimentally demonstrated its application to the induction motor. A better cooling design can improve the motor efficiency, as well as the motor operational reliability [10–12]. In the last decade, thermal analysis play an important role in the design of electrical machines and the use of software devoted to this function has become more and more popular [13–17]. Therefore, it is necessary to optimize thermal management and motor cooling systems to increase the longevity and reliability of the motor [18].

Because of numerous simultaneously active thermal exchanges, the thermal phenomena inside an electrical motor are very complex. Actually, conduction, natural convection, forced convection and radiation are all present with relative weight dependent on the motor cooling system such as natural convection, fan cooling, liquid cooling, etc. In addition, many heat sources are active at the same time. As a consequence, it is difficult to separate the causes and effects in thermal exchange phenomena. Inamura et al. [19] used finite-element analysis (FEM) to study the temperature rise due to core and copper loss in SRM. In their analysis, the energy equation is coupled with loss distribution calculated by 2D FEM. Their results showed that the consideration of temperature rise of inside air in SRM is necessary for more accurate calculations. Chang et al. [20] experimentally and numerically investigates the thermal performance of a large-scale motor with a capacity of 2350 kW. Their models of the fan and motor have been implemented in a Fluent software package to predict the flow and temperature fields inside the motor. Their results showed good agreement with the measured data. Srinivas and Arumugam [21] reported on the thermal analysis carried out on a switched reluctance motor (SRM) by finite element (FE) methods. In their study, thermal flux plot, the isothermal distribution, thermal gradients in different parts of SRM at its different rotor positions and the respective governing equation are presented. Li [22] presented a thermal fluid analysis on the air cooling of a permanent magnet electric motor with a centrifugal impeller numerically and experimentally. In their findings, the cooling flow rate is proportional to the motor rotation speed and cooling is a determining factor for the motor torque rating. In addition, the increase of cooling flow rate does not have significant effect on the convection heat transfer coefficient.

With literatures cited above, it is shown that the importance of estimation heat generation for motor performance. The motor performance is strongly reduced by the temperature rise of the motor. It is necessary to establish a simulated model in designing a motor. However, it is noted CAE design using core and copper loss in SRM is not specified with heat generation in the literatures. In present study, a numerical analysis for SRM operation has been carried out to estimate the iron loss and winding copper loss in advance. The thermal analysis of the SRM is then conducted with consideration of heat generation for the iron and copper loss.

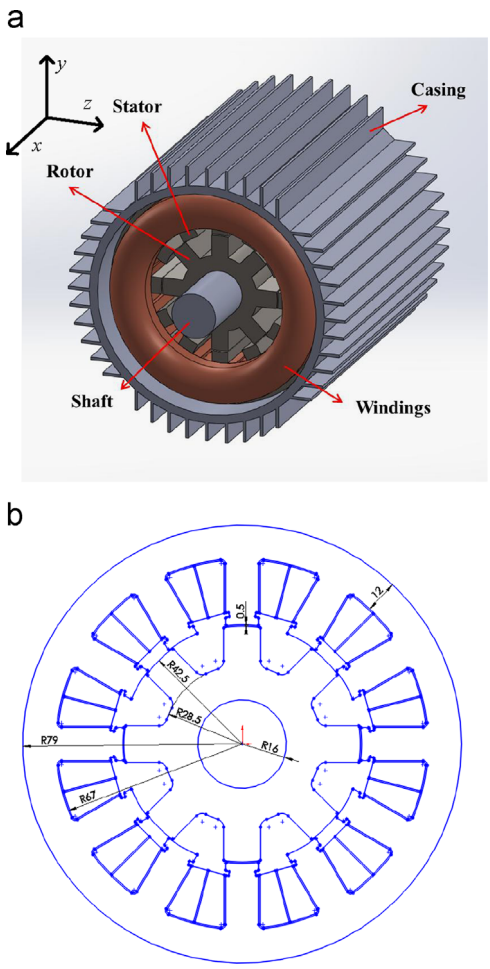

Fig. 1. Structure and dimensions of the switched reluctance motor.

2. Electromagnetic analysis

The structure of a switched reluctance motor shown in Fig. 1(a) includes: a stator, a rotor, a shaft, coil winding and casing. In this study, switched reluctance motor of a golf scooter with 12-slot 8-pole rated power of 3 kW is utilized for the analysis, and its dimensions are depicted in Fig. 1(b). The specifications of the switched reluctance motor are shown in Table 1. The switched reluctance motor is operated with the magnetic resistance to produce reluctance torque. In this study, a fixed power supply voltage of 48 V and constant current of 80 A is used to analyze the electromagnetic characteristics of the motor under various operating conditions.

Mathematic models of voltage, torque and mechanical equations for the analysis of SRM are shown in Eqs. (1)–(3).

Table 1
Specification of the switched reluctance motor.

Number of stator slots		12
Number of poles		8
Number of phases		3
Phase resistance of the coil (Ω)		0.005
Number of turns		7
Copper space factor		76%
Rated power (kW)		3
Rated rotational speed (rpm)		2400
Rotational speed (rpm)		1800–3600
Power supply DC	Voltage (V)	48
	Excitation	Single phase

Table 2
Power losses for each device at various rotational speed.

Rotational speed (rpm)	1800	2100	2400	2700	3000	3300	3600
P_{stator} (W)	73.8	71.2	69.2	67.1	65.6	63.6	62.0
P_{rotor} (W)	69.2	67.9	66.4	67.0	63.3	64.1	62.8
P_{copper} (W)	158.4	105.6	82.6	64.8	54.7	45.6	38.4

$$V_x = i_x \cdot R_x + L_x \frac{di_x}{dt} + e_x \tag{1}$$

$$T_e = \sum_{x=a,b,c} \frac{1}{2} {i_x}^2 \frac{dL_{xx}(\theta_r)}{d\theta_r} \tag{2}$$

$$T_e(\theta_r, i_x) = J\frac{d^2\theta_r}{dt^2} + B\frac{d\theta_r}{dt} + T_L = J\frac{d^2\theta_r}{dt^2} + B\omega_r + T_L \tag{3}$$

where V_x is the x-phase voltage, i_x is the x-phase current, R_x is the x-phase coil winding resistance, and L_x is the x-phase inductance of the coil winding section, e_x is the counter electromotive force of the x phase. T_e is the torque produced by the motor, and θ_r is the rotational angle of the motor, J is the rotational momentum of the motor with loading, B is the friction coefficient of the motor with loading, ω_r is the rotational speed, and T_L is the torque of the loading.

The power losses include iron loss, copper loss and friction loss. The iron loss, containing hysteresis loss and eddy-current loss, is the loss due to materials of stator and rotor. The copper loss is the power loss in copper coil winding. The magnetic analysis software is JMAG-Designer, and the calculated power losses for each device in SRM are listed in Table 2. It is noted that when the rotational speed is low, the output torque is higher resulted in a higher copper loss.

3. Heat transfer analysis

In the procedure, SRM model is established with Solidworks, the necessary heat sources are then obtained with the copper loss and iron loss from the magnetic analysis. Commercial software CFD-RC with finite volume method and semi-implicit method for pressure linked equations is used to find the temperature distribution for the motor and the performance of the cooling mechanism. In the analysis, the dimension of the model is the same as the real motor, the coil winding and insulation material are assumed to be uniform for simplification. The effective heat transfer coefficient is calculated by considering the volume ratio of cooper wire with respect to insulation material. Other assumptions are listed below:

1. Newtonian fluid.
2. Incompressible fluid.
3. No-slip condition.
4. Constant properties.

The governing equations of conservation of continuity, momentum and energy for the fluid are

$$\frac{\partial u}{\partial x} + \frac{\partial v}{\partial y} + \frac{\partial w}{\partial z} = 0 \tag{4}$$

$$\rho_f \left(u\frac{\partial u}{\partial x} + v\frac{\partial u}{\partial y} + w\frac{\partial u}{\partial z} \right) = -\frac{\partial p}{\partial x} + \mu_f \left(\frac{\partial^2 u}{\partial x^2} + \frac{\partial^2 u}{\partial y^2} + \frac{\partial^2 u}{\partial z^2} \right) \tag{5}$$

$$\rho_f \left(u\frac{\partial v}{\partial x} + v\frac{\partial v}{\partial y} + w\frac{\partial v}{\partial z} \right) = -\frac{\partial p}{\partial y} + \mu_f \left(\frac{\partial^2 v}{\partial x^2} + \frac{\partial^2 v}{\partial y^2} + \frac{\partial^2 v}{\partial z^2} \right) \tag{6}$$

$$\rho_f \left(u\frac{\partial w}{\partial x} + v\frac{\partial w}{\partial y} + w\frac{\partial w}{\partial z} \right) = -\frac{\partial p}{\partial z} + \mu_f \left(\frac{\partial^2 w}{\partial x^2} + \frac{\partial^2 w}{\partial y^2} + \frac{\partial^2 w}{\partial z^2} \right) \tag{7}$$

$$\rho_f C_{p,f} \left(u\frac{\partial T_f}{\partial x} + v\frac{\partial T_f}{\partial y} + w\frac{\partial T_f}{\partial z} \right) = k_f \left(\frac{\partial^2 T_f}{\partial x^2} + \frac{\partial^2 T_f}{\partial y^2} + \frac{\partial^2 T_f}{\partial z^2} \right) \tag{8}$$

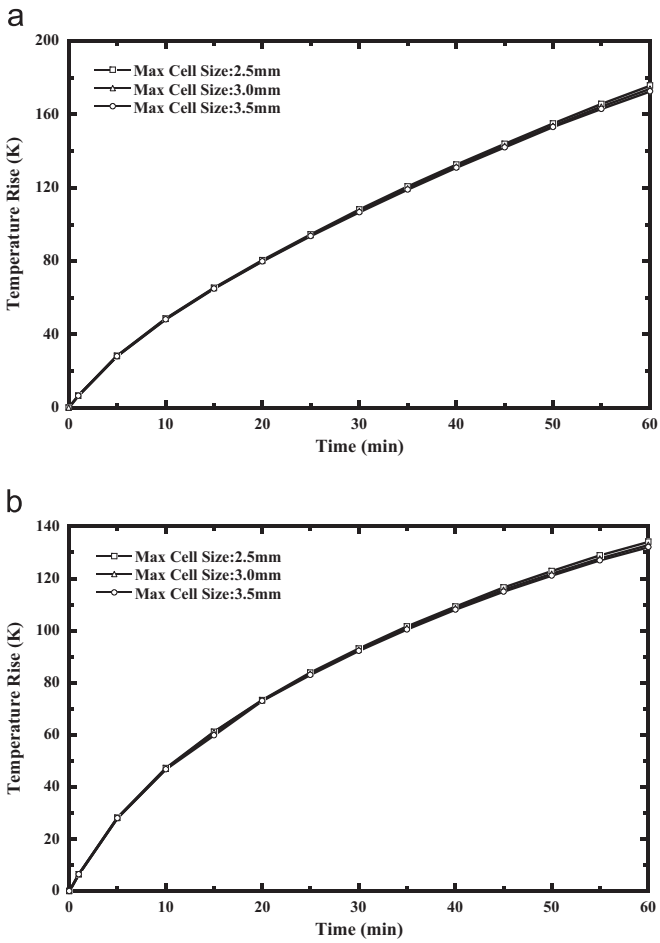

Fig. 2. Comparison of temperature rise with various cell sizes: (a) without cooling casing; (b) with cooling casing.

where p is the pressure, ρ_f is the density of the working fluid, μ_f is the absolute viscosity of the working fluid, $C_{p,f}$ is the specific heat of the working fluid, and k_f is the thermal conductivity of the working fluid. The energy equation for the solid is

$$\rho_s C_{p,s} \frac{\partial T_s}{\partial t} = k_s \left(\frac{\partial^2 T_s}{\partial x^2} + \frac{\partial^2 T_s}{\partial y^2} + \frac{\partial^2 T_s}{\partial z^2} \right) + \dot{q} \tag{9}$$

And ρ_s is the density of the solid, $C_{p,s}$ is the specific heat of the solid, k_s is the conductivity of the solid and $\dot{q}$ is the heat

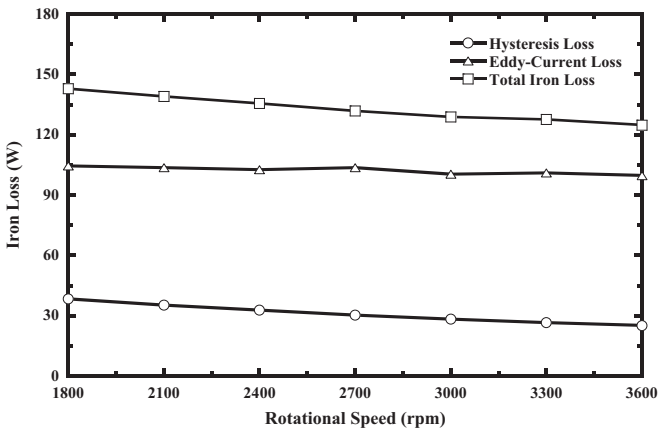

Fig. 3. Effect of rotational speed on the iron loss for a switched reluctance motor with power supply of 48 V.

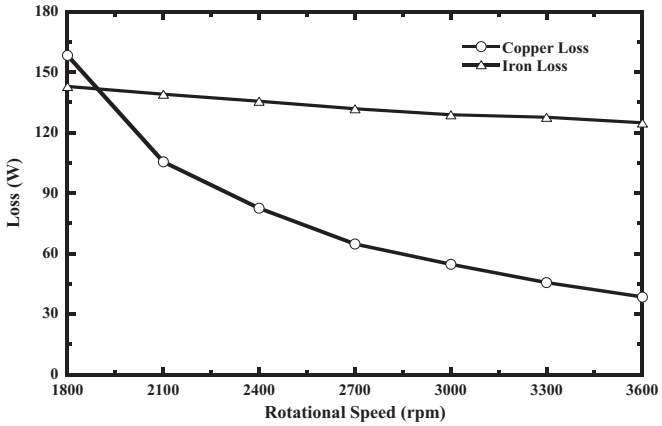

Fig. 4. Effect of rotational speed on the iron loss and copper loss for a switched reluctance motor with power supply of 48 V.

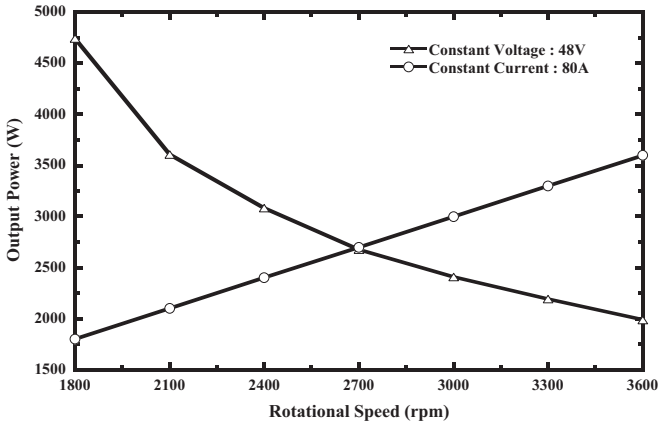

Fig. 5. Effect of rotational speed on the output power for constant current and voltage power supply for a switched reluctance motor.

generation rate per solid volume.

The interfaces between fluid and solids are constant temperature, as well as the interface between solids. For the outside cooling of the motor, due to no-slip condition, the heat flux can be expressed as

$$-k\frac{\partial T}{\partial x} = h_{out}\,(T_{s,out} - T_{f,out}) \tag{10}$$

where $T_{s,out}$ is the wall temperature outside the motor, and $T_{f,out}$ is the ambient temperature of air. For the cooling inside motor, h_{in} is given for the cooling velocity, the cooling heat flux is given as

$$-k\frac{\partial T}{\partial x} = h_{in}\,(T_{s,in} - T_{f,in}) \tag{11}$$

where $T_{s,in}$ is the wall temperature inside the motor, and $T_{f,in}$ is the inside air temperature. For natural convection, $h = 10$ W/m^2 K; for forced convection, $h = 10$–100 W/m^2 K.

In this study, the rated power of the switched reluctance motor is 3 kW with air-cooled heat sink design. The cooling fin on the outside of the motor housing is made of aluminum and to increase the convection heat transfer surface. The fin configurations are shown in Fig. 1. The motor housing is 6 mm in thickness and 210 mm in length. The fin width is 2 mm in width and 15 mm in height.

4. Numerical methods

In the magnetic analysis, FEM with Fast Fourier Transform (FFT) is used to calculate the power loss, the grid points are generated with designated cell sizes. As for the heat transfer analysis, finite volume method with unstructured grid is utilized for the simulation. Convergence requirement is set to be less than 10^{-6} for iteration. The cell size in the gap between stator and rotor is set as at 0.5 mm, and cell sizes for the solid parts are set at 1 mm, 2 mm, and 3 mm, respectively

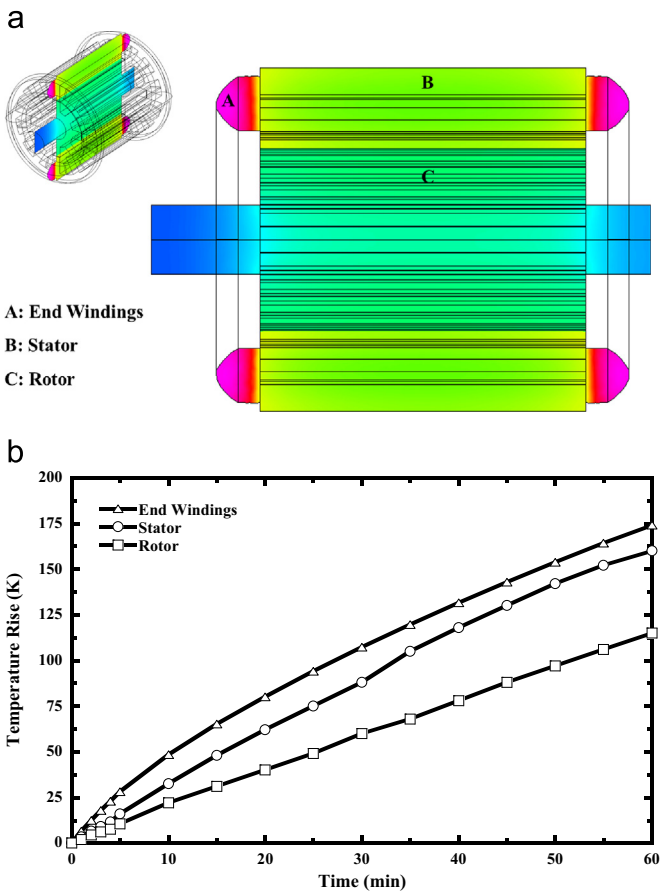

Fig. 6. (a) Schematic diagram of cross-sectional temperature distribution; and (b) transient temperature plot for SRM without cooling casing at 2400 rpm.

for comparison in cell size dependence. It is found that the power losses for each case are within 0.2%.

In the heat transfer analysis, due to large variation in heat conduction between solid and fluid, the minimum cell size is 0.004 mm for the fluid close to solid surfaces, and the maximum cell size is set at 2.5 mm, 3 mm, and 3.5 mm, respectively for grid size investigation. Results are presented in Fig. 2. It is observed that the differences of temperature rises for copper wire are within 0.8%. Although increase grid point in the analysis will obtain a more accurate solution, it will be time consuming as well. In this present study, the cell size is set at 2 mm for magnetic analysis. As for the heat transfer analysis, the maximum cell size is 3 mm and the minimum cell size is 0.004 mm. The total grid points are 387,388 for model without cooling casing and 532,073 for model with cooling casing.

5. Results and discussion

In present study, both magnetic and heat transfer analyzes have been performed for the SRM. Numerical simulation on the losses generated by the coil windings of the switched reluctance motor has been conducted for the heat source in heat transfer analysis. Fig. 3 shows the effect of rotational speed on the overall hysteresis loss and eddy current loss in a switched reluctance motor. It is seen that the overall losses decreases as rotational speed increases for a constant voltage supply of 48 V. However, the decrease is relative small. This is because the higher the rotational speed, the higher the commutation frequency, the smaller the excitation current, in turns a smaller maximum flux density. The effect of rotational speed on the iron loss and copper loss rotor is presented in Fig. 4. It is found that both iron loss and copper loss decrease as rotational speed increases. It is obvious that the decrease in copper loss is significant with higher rotational speed. This is due to low magnetized current with higher rotational speed of lower torque resulting in a smaller low copper loss. Fig. 5 presents the output power as a function of rotational speed for constant current and voltage power supply conditions. It is depicted that the output power is almost a linear relation to the rotational speed at constant current supply. On the other hand, the power output is less for higher rotational speed at constant voltage power supply, since the power output is under the influence of excited current, such that the output torque becomes less.

After electromagnetic analysis, the power loss is considered as the heat source for temperature field calculation.

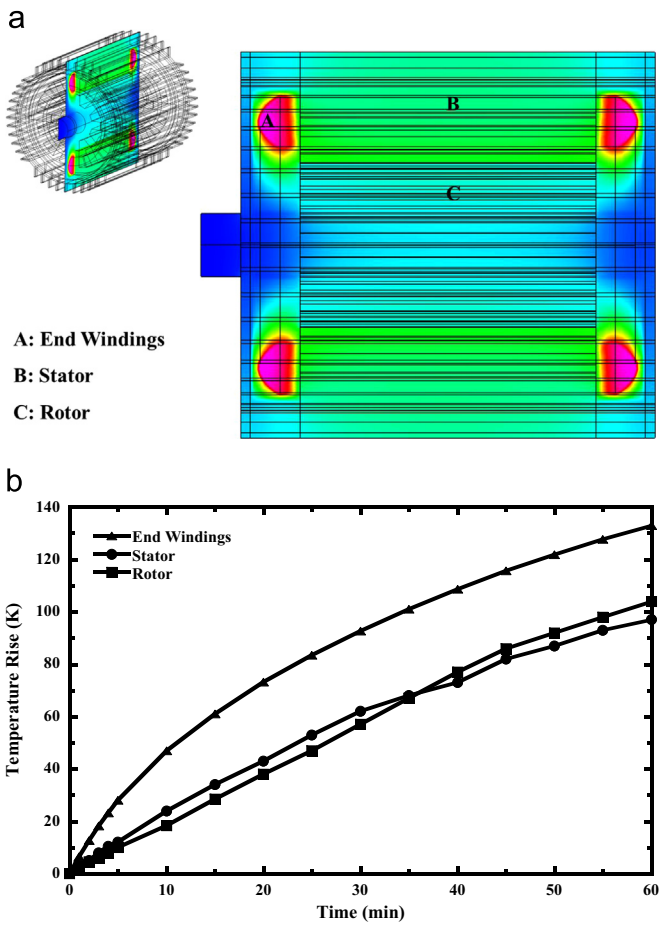

Fig. 7. (a) Schematic diagram of cross-sectional temperature distribution; and (b) transient temperature plot for SRM with cooling casing at 2400 rpm.

Figs. 6 and 7 show the estimated temperature for each components verse time in a SRM without and with cooling casing, respectively. It is observed that the temperature of end winding is the highest among these components. This is because end winding is the main heat source inside the motor. It is also noticed that the temperatures with cooling casing is always lower than those without cooling casing. Actually, the temperature rise of end winding should not exceed more than 80 K. If the temperature rise of end winding exceeds 80 K, end winding would be broken due to overheating. This indicates that SRM without cooling casing can be operated less than 20 min at the operating condition. However, SRM with cooling casing can be operated about 23 min. This is because the heat is conducted outwards with contact of stator and cooling casing.

Temperature distributions inside SRM with and without cooling casing for both XY and YZ central plane have been found and presented in Fig. 8. It is noted that the end-winding temperature is independent to the installing of cooling casing. However, the temperature of the stator decreases with a cooling casing. It is also found that the high temperature located in stator and end winding zones from Fig. 8(c) and (d). Through the analysis, the temperature rise of the end winding in the SRM is greater than that of stator and rotor in rotational speed of 2400 rpm without any cooling design for natural convection. For the given condition of temperature rise less than 80 K, it takes less than 20 min for the end winding to become short due to overheating. However, the time of the end winding becoming short is predicted to be 23 min with a cooling casing for the SRM.

Fig. 9 shows the temperature rise as a function of time for end winding, stator, and rotor of the SRM with and without cooling casing with rotational speed of 2400 rpm. It is observed that the temperature rises of these three components are improved with a cooling casing. For the 10th minute of the SRM operation, the temperature rises are lower 1.5 K, 8.5 K and 3.6 K for end winding, stator, and rotor, respectively. The effective cooling performances for each component with a cooling casing are enhanced by 3.1%, 26.1%, and 16.4%, respectively. The forced convection conditions are discussed in Fig. 10. The convection heat transfer coefficients are taken as 20, 40 and 80 W/m^2 K to study the cooling performance of a SRM with a cooling casing. It is obvious that the temperature decreases as h_{out} increases. Since the convection effect is better, and the temperature of the end winding decreases 0.8, 2.1 and 3.8 K for h_{out} is 20, 40, and 80 W/m^2 K, respectively, comparing to that of $h_{out}=10$ W/m^2 K for natural convection. The cooling performance for end winding increases approximately from 1.7% to 8%. As for the stator, the cooling performance increases about 8–40%. The study of installing an internal fan with blade

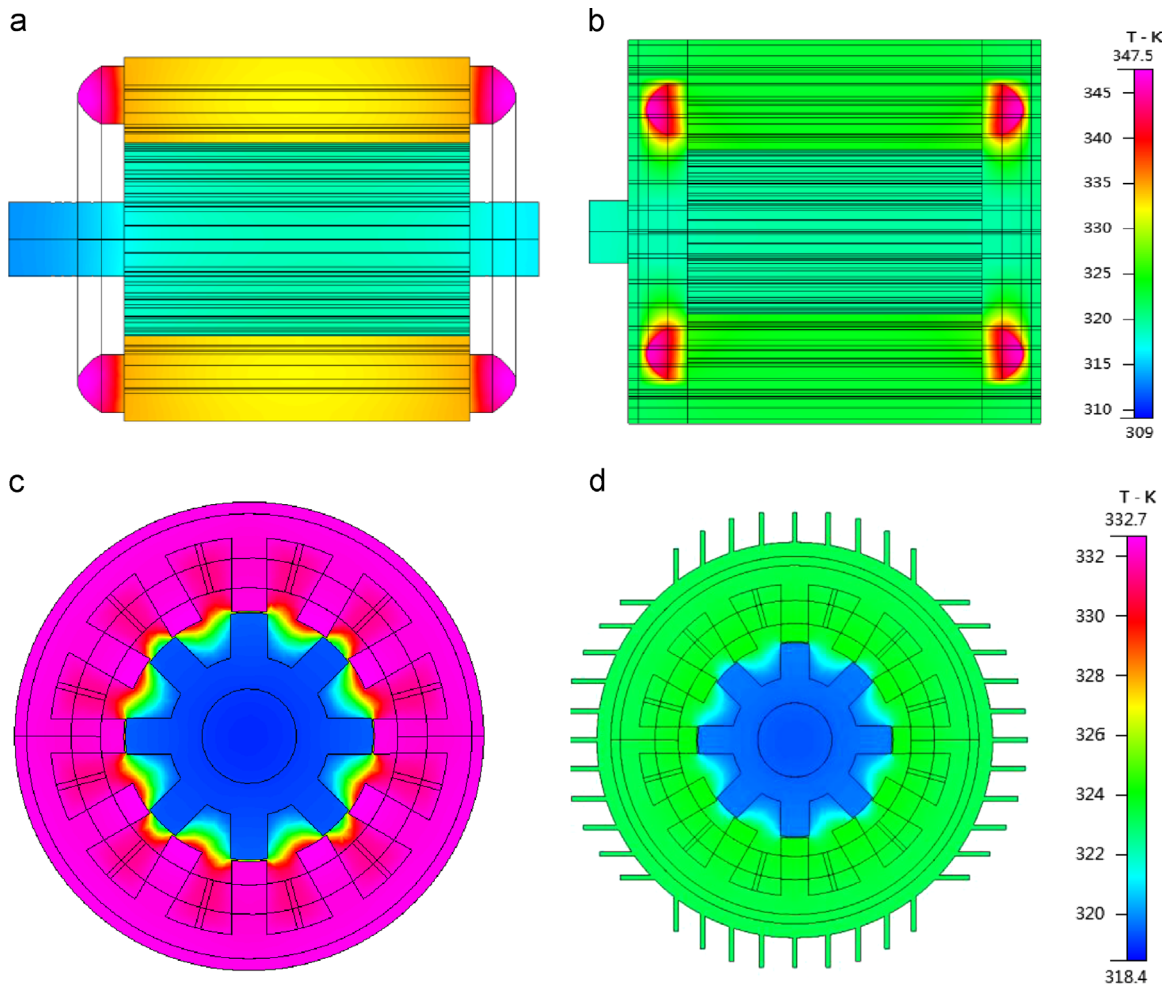

Fig. 8. Temperature distributions for (a) without cooling casing in XY plane; (b) with cooling casing in XY plane; (c) without cooling casing in YZ plane; (d) with cooling casing in YZ plane in a SRM with rotational speed of 2400 rpm in the operation of the 10th minute for natural convection as $h_{out}=10\ \mathrm{W/m^2\ K}$.

diameter of 84 mm has been conducted in the analysis. Fan blade rotates in the same speed as the motor, and the air speed is used for the internal cooling in the motor. Fig. 11 presents the temperature distributions in XY plane with and without internal fan with cooling casing in a SRM at 2400 rpm for the 10th minute of operation for $h_{out}=40\ \mathrm{W/m^2\ K}$. It is found that the end winding temperature decreases approximately 7 K. The improvement of cooling performance is estimated about 17.5%. This indicates the cooling performance is enhanced by installation of internal fan.

6. Conclusions

In this paper, both electromagnetic field and temperature field of a switched reluctance motor have been analyzed. Commercial software of JMAG and CFD-RC and used for electromagnetic and temperature fields, respectively. The energy loss of conversion from electricity to magnetic torque is considered as the heat generation in the temperature field. Brief summaries are drawn as below:

1. The overall power loss decreases as rotational speed increases for a constant voltage supply of 48 V. However, the decrease is relative small. This is because higher rotational speed results in higher commutation frequency and smaller excitation current, in turns a smaller maximum flux density.
2. Both iron loss and copper loss decrease as rotational speed increases. The reduction of copper loss is more significant due to higher starting torque with larger current at lower rotational speed for constant voltage power supply of 48 V.
3. For constant current power supply condition, the output power is almost a linear relation to the rotational speed; while the power output is less for higher rotational speed at constant voltage power supply condition.

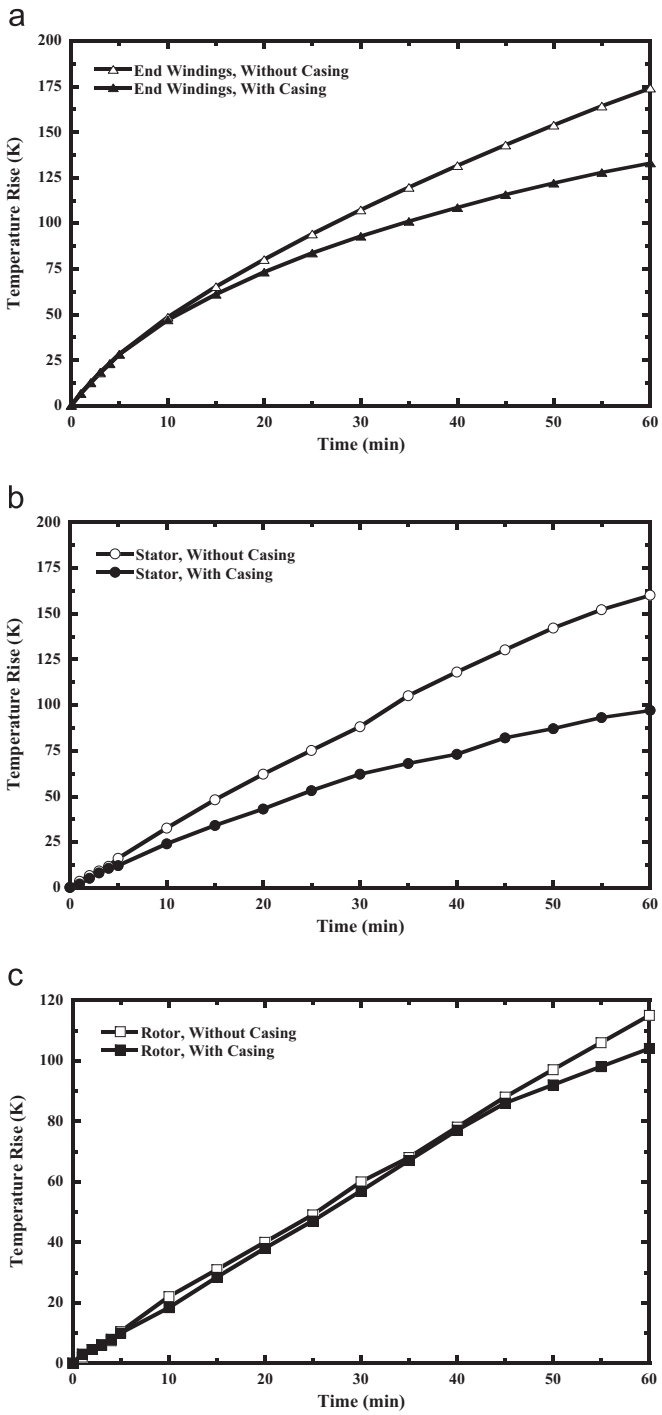

Fig. 9. Average temperature rise as a function of time with and without cooling casing for (a) end windings; (b) stator; and (c) rotor.

4. According to the numerical analysis, if there is no any cooling design, the ending winding of the SRM will be damaged due to overheating in 20 min at the rotational speed of 2400 rpm.
5. The cooling performance of SRM with cooling casing is improved by 26.1%, 16.4%, and 3.1% for stator, rotor, and end winding, respectively under natural convection condition. In addition, cooling performance is enhanced approximately 1.7–8% for end winding under external forced convection. Also, internal fan raises cooling on the end winding by 17.5%.

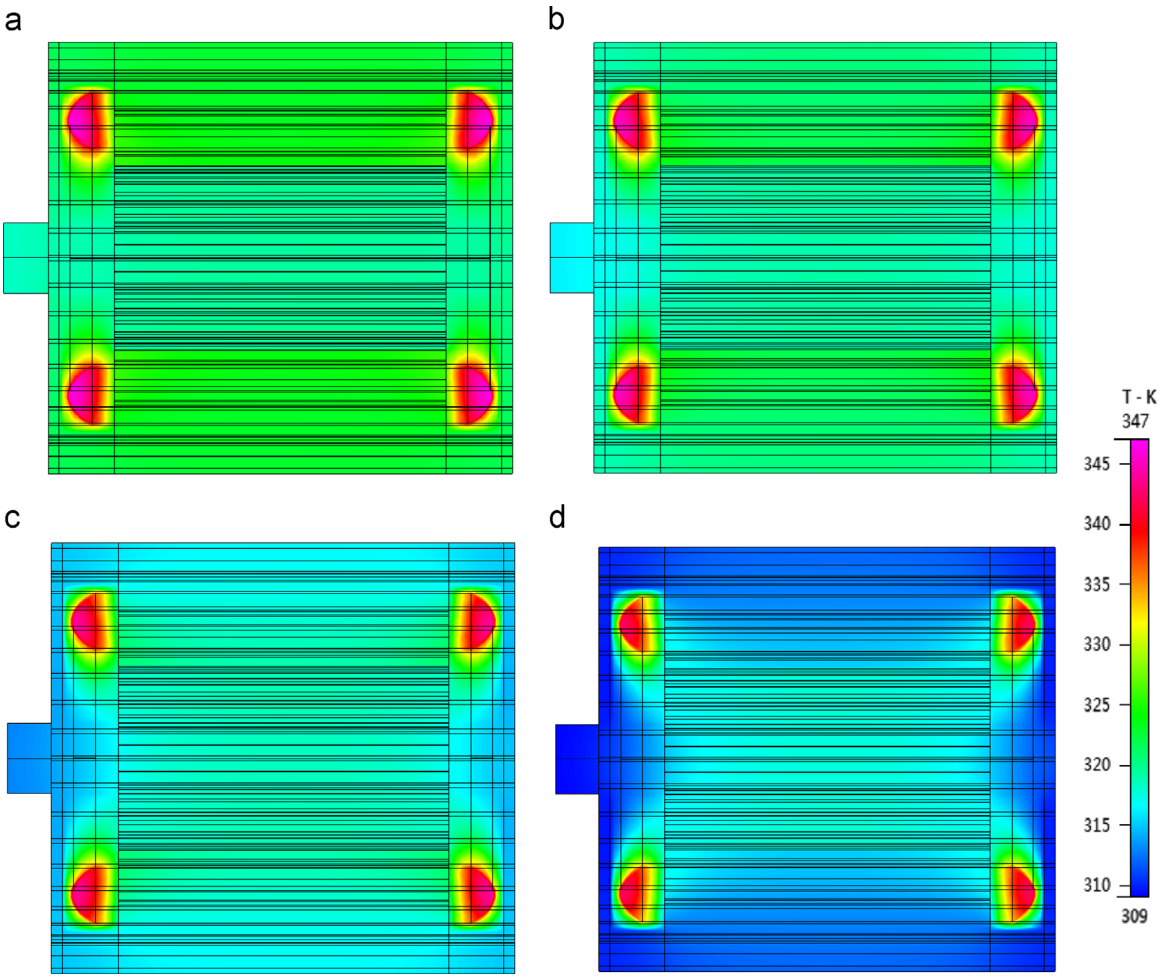

Fig. 10. Temperature distributions for (a) h_{out}=10 W/m^2 K; (b) h_{out}=20 W/m^2 K; (c) h_{out}=40 W/m^2 K; (d) h_{out}=80 W/m^2 K with cooling casing in a SRM with rotational speed of 2400 rpm in the operation of the 10th minute.

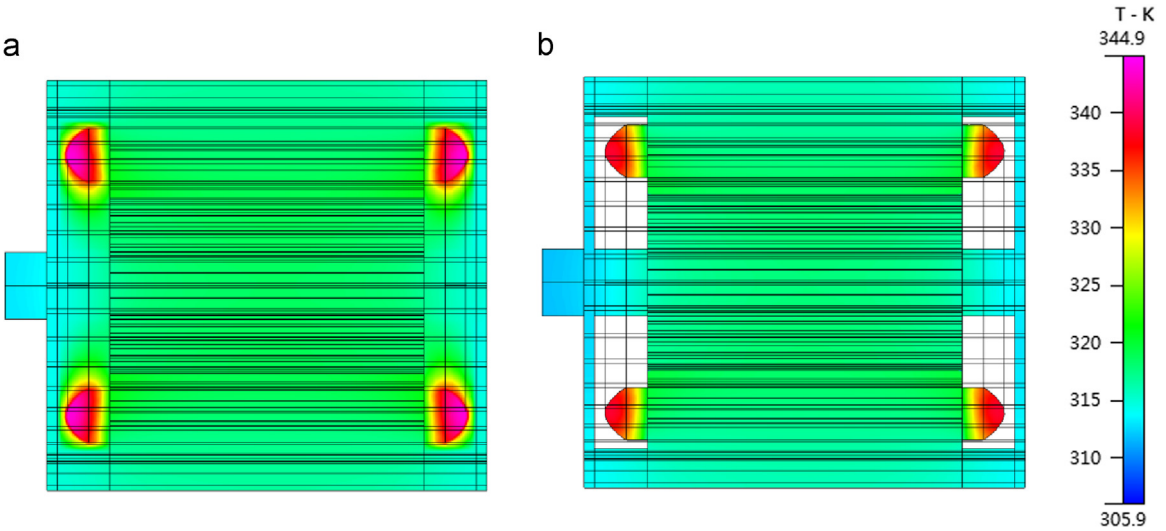

Fig. 11. Temperature distributions in YZ plane (a) without internal fan and (b) with internal fan with cooling casing in a SRM with rotational speed of 2400 rpm in the operation of the 10th minute.

Acknowledgment

The financial support by the Ministry of Science and Technology, R.O.C., through the contract MOST 101-2221-E-027-149-MY2 is highly appreciated.

References

[1] K.M. Rahman, B. Fahimi, G. Suresh, A.V. Rajarathnam, M. Ehsani, Advantages of switched reluctance motor applications to EV and HEV: design and control issues, IEEE Trans. Ind. Appl. 36 (2000) 111–121.
[2] K. Nakamura, S. Fujio, O. Ichinokura, A method for calculating iron loss of an SR motor based on reluctance network analysis and comparison of symmetric and asymmetric excitation, IEEE Trans. Magn. 42 (10) (2006) 3440–3442.
[3] K. Ohyama, M.N.F. Nashed, K. Aso, H. Fujii, H. Uehara, Design using finite element analysis of a switched reluctance motor for electric vehicle, in: Proceedings of the Second Conference on Information and Communication Technologies, ICTTA '06, 2006, pp. 727– 732.
[4] N.N. Fulton, The application of CAD to switched reluctance drives, in: Proceedings of the IEEE Conference on Electric Machines and Drives, 1987, pp. 275–279.
[5] T.J.E. Miller, M. McGilp, Nonlinear theory of the switched reluctance motor for rapid computer-aided design, Proc. Inst. Elect. Eng. 137B (6) (1990) 337–347.
[6] A. Kakilli, Magnetic analysis of modified-rotor switched reluctance motor, Electron. Electr. Eng. 115 (9) (2011) 21–26.
[7] G.J. Li, J. Ojeda, E. Hoang, M. Lecrivain, M. Gabsi, Comparative studies between classical and mutually coupled switched reluctance motors using thermal-electromagnetic analysis for driving cycles, IEEE Trans. Magn. 47 (4) (2011) 839–847.
[8] J.R.M. Szogyen, Cooling of electric motors, IEE J. Elect. Power Appl. 2 (2) (1979) 59–67.
[9] J. Faiz, R. Iranpour, P. Pillay, Thermal model for a switched reluctance motor of TEFC design during steady and transient operation, Electr. Mach. Power Syst. 26 (1) (1998) 77–91.
[10] M.K. Yoon, C.S. Jeon, S.K. Kauh, Efficiency increase of an induction motor by improving cooling performance, IEEE Trans. Energy Convers. 17 (1) (2002) 1–6.
[11] J.K. Woodard, G.E. Johnson, Optimal design of cooling fans for industrial electric motors, J. Mech. Transm. Autom. Des. 108 (2) (1986) 224–225.
[12] T. Nakahama, D. Biswas, K. Kawano, F. Ishibashi, Improved cooling performance of large motors using fans, IEEE Trans. Energy Convers. 21 (2) (2006) 324–331.
[13] I. Boldea, S.A. Nasar, The Induction Machine Handbook, CRC Press, Hoboken, NJ, 2002.
[14] A. Boglietti, Guest editorial of the special section on thermal issues in electrical machines and drives, Trans. Ind. Electron. 55 (10) (2008) 3498–3499.
[15] W. Wei, J.B. Dunlop, S.J. Collocott, B.A. Kalan, Design optimization of a switched reluctance motor by electromagnetic and thermal finite-element analysis, IEEE Trans. Magn. 39 (2003) 3334–3336.
[16] A. Boglietti, A. Cavagnino, D. Staton, M. Shanel, M. Mueller, C. Mejuto, Evolution and modern approaches for thermal analysis of electrical machines, Trans. Ind. Electron. 56 (3) (2009) 871–882.
[17] J. Faiz, A. Dadgari, Heat distribution and thermal calculations for switched reluctance motors, in: Proceedings of the Fifth International Conference on Electrical Machines and Drives, 1991, pp. 305–310.
[18] A.H. Bonnett, Operating temperature considerations and performance characteristics for IEEE 841 motors, IEEE Trans. Ind. Appl. 37 (2001) 1120–1131.
[19] S. Inamura, T. Sakai, K. Sawa, A temperature rise analysis of switched reluctance motor due to the core and copper loss by FEM, IEEE Trans. Magn. 39 (3) (2003) 1554–1557. 2003.
[20] C.C. Chang, Y.F. Kuo, J.C. Wang, S.L. Chen, Air cooling for a large-scale motor, Appl. Thermal Eng. 30 (2010) 1360–1368.
[21] K.N. Srinivas, R. Arumugam, Thermal characterization through finite element analysis of the switched reluctance motor, TENCON 2001, in: Proceedings of IEEE Region 10 International Conference on Electrical and Electronic Technology, 2001, pp. 819–823.
[22] H. Li, Cooling of a permanent magnet electric motor with a centrifugal impeller, Int. J. Heat Mass Transf. 53 (2010) 797–810.